Search for heavy neutrinos in $\pi \to \mu\nu$ decay

A. Aguilar-Arevalo [a], M. Aoki [b], M. Blecher [c], D.I. Britton [d], D. vom Bruch [e,1], D.A. Bryman [e,f], S. Chen [g], J. Comfort [h], L. Doria [f,2], S. Cuen-Rochin [e,f], P. Gumplinger [f], A. Hussein [i,f], Y. Igarashi [j], S. Ito [b,*,3], S.H. Kettell [k], L. Kurchaninov [f], L.S. Littenberg [k], C. Malbrunot [e,4], R.E. Mischke [f], T. Numao [f,*], D. Protopopescu [d], A. Sher [f], T. Sullivan [e,5], D. Vavilov [f]

[a] Instituto de Ciencias Nucleares, Universidad Nacional Autónoma de Mexico, D.F. 04510, Mexico
[b] Graduate School of Science, Osaka University, Toyonaka, Osaka 560-0043, Japan
[c] Physics Department, Virginia Tech., Blacksburg, VA 24061, USA
[d] School of Physics and Astronomy, University of Glasgow, Glasgow, G12 8QQ, UK
[e] Department of Physics and Astronomy, University of British Columbia, Vancouver, British Columbia, V6T 1Z1, Canada
[f] TRIUMF, 4004 Wesbrook Mall, Vancouver, British Columbia, V6T 2A3, Canada
[g] Department of Engineering Physics, Tsinghua University, Beijing, 100084, China
[h] Physics Department, Arizona State University, Tempe, AZ 85287, USA
[i] University of Northern British Columbia, Prince George, British Columbia, V2N 4Z9, Canada
[j] KEK, 1-1 Oho, Tsukuba-shi, Ibaraki 305-0801, Japan
[k] Brookhaven National Laboratory, Upton, NY 11973-5000, USA

ARTICLE INFO

ABSTRACT

In the present work of the PIENU experiment, heavy neutrinos were sought in pion decays $\pi^+ \to \mu^+\nu$ at rest by examining the observed muon energy spectrum for extra peaks in addition to the expected peak for a light neutrino. No evidence for heavy neutrinos was observed. Upper limits were set on the neutrino mixing matrix $|U_{\mu i}|^2$ in the neutrino mass region of 15.7–33.8 MeV/c^2, improving on previous results by an order of magnitude.

© 2019 The Authors. Published by Elsevier B.V. This is an open access article under the CC BY license (http://creativecommons.org/licenses/by/4.0/). Funded by SCOAP^3.

1. Introduction

Neutrino oscillations indicate that at least two of the known neutrinos are massive, requiring the original Standard Model to be expanded. The existence of additional heavy neutrinos (mostly sterile, without direct coupling in weak interactions) is still an open question. A wide range of motivations [1] for sterile neutrinos come from cosmological and astrophysical arguments of baryogenesis [2], large scale structure formation [3] and big bang nucleosynthesis [4], and from the tension in the Hubble constant [5]. In the Neutrino Minimal Standard Model (νMSM) three sterile neutrinos are introduced which include a stable dark matter candidate [6]. MeV neutrinos could be accommodated in the νMSM to explain the ^{7}Li abundance [7] or, with the addition of a MeV scalar, to obtain consistent results for anomalies in neutrino experiments [8]. In many scenarios, the mass scale of sterile neutrinos is not constrained to be light [9,10], opening up many possibilities and potential observables in particle physics, astrophysics and cosmology.

Heavy neutrinos mixing with the muon neutrino in the mass region 1–400 MeV/c^2 have been sought by accelerator-based experiments studying pion [11–14] and kaon decays [15–17]. The ratio of the $\pi^+ \to \mu^+\nu_H$ decay rate to the normal $\pi^+ \to \mu^+\nu$ decay rate can be written as

$$\frac{\Gamma(\pi^+ \to \mu^+\nu_H)}{\Gamma(\pi^+ \to \mu^+\nu)} = |U_{\mu i}|^2 \bar{\rho}(m_H) \qquad (1)$$
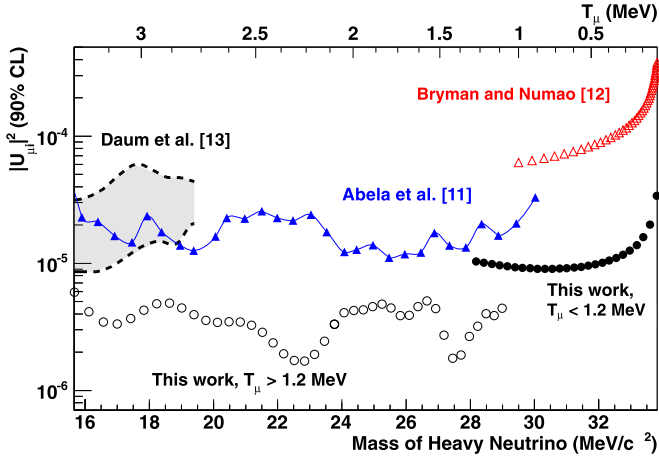
Fig. 1. Summary of 90% CL upper limits on $|U_{\mu i}|^2$ vs m_H. The upper scale shows muon kinetic energy. The closed blue and open red triangles indicate the previous limits by [11] and [12], respectively. Upper limits by [13] are located in the shaded region between the two dashed lines. The closed black circles are the results of the present work for the region $0 < T_\mu < 1.2$ MeV and the open black circles for the region $1.1 < T_\mu < 3.3$ MeV.

for $|U_{\mu i}|^2 << 1$, where m_H is the mass of the heavy neutrino ν_H, $\overline{\rho}(m_H)$ accounts for the phase space and helicity suppression factors (normalized to the zero-mass neutrino case) [18], and $U_{\mu i}$ is the neutrino mixing parameter for the weak muon-neutrino eigenstate ν_μ and the mass eigenstate ν_i.

Using stopped pions in an active detector, Abela et al. [11] measured the kinetic energy of muons from the decay $\pi^+ \rightarrow \mu^+\nu$ (kinetic energy $T_\mu = 4.1$ MeV for a massless neutrino), and searched for low-energy peaks due to heavy neutrinos. Upper limits on $|U_{\mu i}|^2$ for the 5–30 MeV/c^2 region were set at a level of 10^{-2}–10^{-5}; the experiment was limited by accidental background. Heavy neutrinos in the mass region 30–33.9 MeV/c^2 were also sought in pion decay by Bryman and Numao [12], providing upper limits of 10^{-3}–10^{-4}; this search was limited by background coming from pion decays in flight (πDIF). Daum et al. [13] employed a similar technique but with excellent energy resolution (~ 10 keV) using a Germanium detector; the search region was 1-20 MeV/c^2 with a sensitivity level of 10^{-5}, which was limited by statistics. A dedicated magnetic spectrometer experiment [14] searched for a 33.9 MeV/c^2 neutrino, providing a limit of a 10^{-8} level on $|U_{\mu i}|^2$. Fig. 1 shows a summary of the present status of the search for heavy neutrinos at 90% confidence level (CL) in the mass region 15.7–33.8 MeV/c^2.

The present search for heavy neutrinos was based on measurement of the muon kinetic energy in $\pi^+ \rightarrow \mu^+\nu$ decays at rest. When a pion is stopped in a thick plastic scintillator all decay vertices are contained; the first signal is from the kinetic energy of the incident beam pion, the second from the muon in $\pi^+ \rightarrow \mu^+\nu$ decay, and the third from the positron in $\mu^+ \rightarrow e^+\nu\overline{\nu}$ decay ($\pi^+ \rightarrow \mu^+ \rightarrow e^+$ decay); the positron usually escapes in the case considered here. In the present study, the leading backgrounds arising from accidental particles and πDIF were suppressed using waveform and tracking information to identify extra activity in the detector system, and the statistics were improved by an order of magnitude over previous experiments.

2. Experiment

The present search was carried out as a part of the PIENU experiment [19], a measurement of the branching ratio $\Gamma(\pi^+ \rightarrow e^+\nu(\gamma))/\Gamma(\pi^+ \rightarrow \mu^+\nu(\gamma))$ using pion decays at rest, where (γ) indicates inclusion of radiative processes.
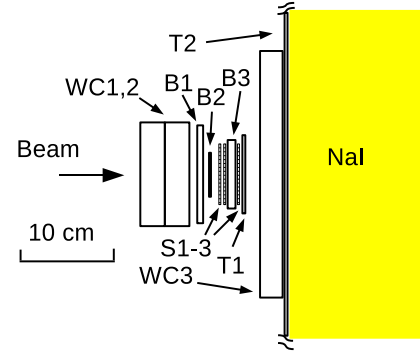

Fig. 2. Cross-sectional view of the PIENU detector. CsI detectors surrounding the NaI crystal are not shown here.

Fig. 2 shows a schematic view of the PIENU apparatus [20]. A 75-MeV/c π^+ beam from the TRIUMF M13 channel [21] was detected by WC1 and WC2 (wire chambers), B1 and B2 (plastic scintillators), and S1 and S2 (silicon strip detectors), and stopped in an 8-mm thick plastic scintillator target (B3) at a rate of 5×10^4 π^+/s. The pion stopping-depth distribution in B3 was centered with the RMS width of 0.7 mm. Independent pion tracking was provided by WC1 and WC2 for the upstream end of the detector system, and by S1 and S2 near B3. Positrons from $\mu^+ \rightarrow e^+\nu\overline{\nu}$ decays in B3 were measured by another X-Y set of silicon strip detectors (S3), two thin plastic scintillators (T1 and T2), a set of wire chambers (WC3), and a calorimeter, consisting of a 48-cm (dia.) $\times$ 48-cm (length) single-crystal NaI(Tℓ) detector [22] surrounded by two concentric layers of pure CsI crystals [23].

A positron signal from muon decay (defined by a T1–T2 coincidence) in a time window between -300 and 540 ns with respect to the incoming pion was the basis of the main trigger with a rate of 3×10^3 s^{-1}. This was scaled down by a factor of 16 to form an unbiased trigger (Prescaled trigger). Other triggers included a positron beam trigger for calibration and ones for enhancing rare $\pi^+ \rightarrow e^+\nu$ decays. The data were taken in 2009-2012. The number of Prescaled-trigger events used in this analysis was 4×10^9.

3. Data processing and event selection

The charge and time of each scintillator pulse were extracted from the waveform recorded by a 500-MHz digitizer [24]. The charge for each pulse was obtained by integrating the pulse from -20 to 20 ns around the local maximum for plastic scintillators B1–3 and T1–2. Also, there were several integration windows for each detector system to accommodate specific purposes described later. Each readout channel was calibrated to the expected energy loss for 75-MeV/c beam particles. The nonlinear response of plastic scintillator was studied in a Monte Carlo (MC) simulation [25] and consistency of calibration was confirmed within 0.1 MeV.

Events originating from pions were selected based on their energy loss in B1 and B2, and the presence of a B3 hit. Events with extra activity other than that of the $\pi^+ \rightarrow \mu^+ \rightarrow e^+$ decay sequence in B1, B2, B3, T1 and T2 within the time region of -6.4 to 1.4 μs with respect to the pion stop were rejected; this reduced the accidental background by more than an order of magnitude.

In order to ensure that an event was due to $\pi^+ \rightarrow \mu^+ \rightarrow e^+$ decay, the calorimeter energy was required to be <55 MeV and a loose geometrical positron acceptance cut (the radius of the hit position at WC3 to be <80 mm) was applied. The number of $\pi^+ \rightarrow \mu^+ \rightarrow e^+$ events was 5×10^8.

A second pulse in B3 due to the muon kinetic energy needed to be identified in the search. However, when the muon energy involving ν_H was below 1.2 MeV the pulse detection logic could
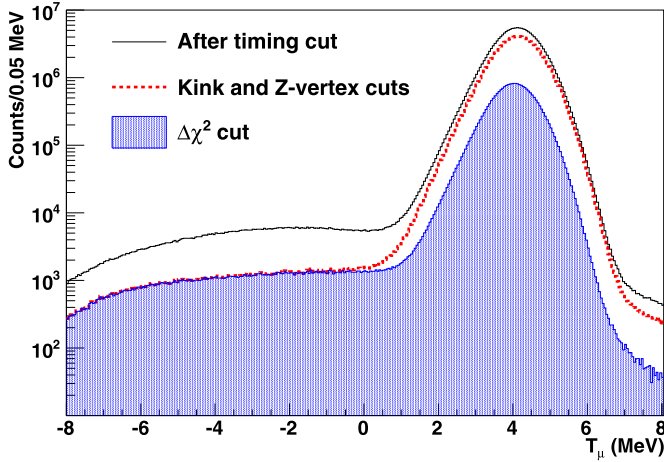
Fig. 3. Energy spectra of muons for the $T_\mu < 1.2$ MeV analysis, after subtraction of pion and positron energies from the total energy, with several cuts; the black line indicates the spectrum after the positron time cut, the dotted red line after the kink and Z vertex cuts, and the shaded blue histogram after the $\Delta\chi^2$ cut.

not efficiently identify the pulse. The search was, therefore, divided into two muon energy regions, above and below 1.2 MeV. In the region below 1.2 MeV the integrated energy in B3 up to 600 ns, which contained the $\pi^+ \to \mu^+ \to e^+$ decay sequence, was examined for the muon energy contribution as described in the following section, while in the region above 1.2 MeV the energy of a cleanly separated second pulse was used. In each analysis, all $\pi^+ \to \mu^+ \to e^+$ decay events were examined.

4. Analysis of the region below 1.2 MeV

Since the B3 energy observed with the wide time window included the pion and positron contributions in addition to the kinetic energy of the muon, these energies were first subtracted.

The contribution from the positron pulse, which resulted in a wider energy distribution due to the path length variation of the positron in B3, was subtracted using a well separated positron pulse in B3. In order not to affect the $\pi^+ \to \mu^+ \nu$ decay measurement, late positron time was required ($300 < t_{T1} - t_{B1} < 500$ ns).

In order to correct for the energy-loss variation of pions in the upstream detectors, the energies of the other beam counters (B1, B2, S1 and S2) were added for this search. Then, the contribution of the average pion kinetic energy (~ 17 MeV) was subtracted from the total energy. The black histogram in Fig. 3 shows the spectrum of the muon energy after the positron and pion energies were subtracted from the total energy. The events in the $T_\mu < 0$ MeV region are due to the main background π DIF occurring very near or in B3, in which the observed "pion plus muon" energy is less than the incident pion beam energy. Another background is due to the low-energy tail of the 4.1 MeV peak extending to $T_\mu = 0$ MeV. The contribution from pion radiative decay $\pi \to \mu\nu\gamma$ is negligible.

The π DIF background was suppressed by two cuts [26]. The angle between the track vectors measured by WC1-2 (upstream) and S1-2 (near B3) provided a measure of a kink in the pion track due to π DIF. Limiting the kink angle suppressed the π DIF background. The muon decay vertex in the beam direction (Z-vertex) obtained from the pion (WC1-2 and S1-2) and positron (S3 and WC3) tracks also allowed identification of π DIF in B3. The effects of these cuts are shown by the red histogram. The low energy tail of the 4.1 MeV peak, mainly due to cleanly separated $\pi^+ \to \mu^+ \to e^+$ decays, was suppressed by a consistency test based on the difference of χ^2 values per degrees of freedom for two- and three-pulse fits. In this $\Delta\chi^2$ cut, only three pulse events with the second pulse
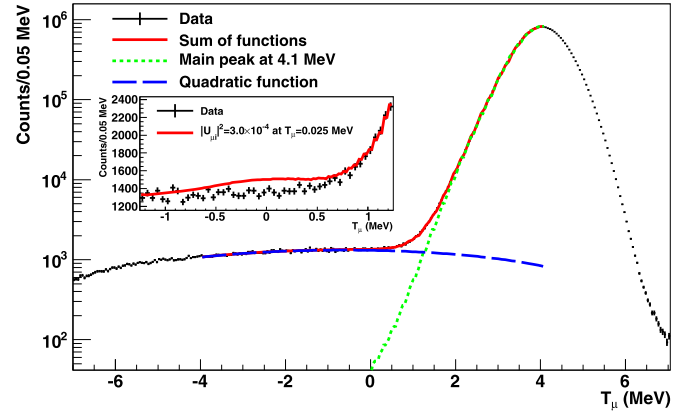

Fig. 4. Fit results for the region $T_\mu < 1.2$ MeV. The black crosses with statistical errors, and the dashed blue and dotted green lines indicate data, quadratic background and the 4.1 MeV peak, respectively. The effect of the broad Gaussian in the fitting function was included. In the insert, the red line indicates a hypothetical signal at 0.025 MeV for $|U_{\mu i}|^2 = 3 \times 10^{-4}$.

falling into $T_{2nd} > 2$ MeV were rejected, so that the acceptance loss for the signal ($T_\mu < 1.2$ MeV) was negligible. After all cuts, the small but dominant background was still from π DIF in B3 as shown by the shaded blue histogram in Fig. 3.

4.1. Fit

There are two background shapes to be reproduced at energies above and below the signal region (0–1.2 MeV): the 4.1 MeV peak and the π DIF shape. The slightly asymmetric shape of the 4.1 MeV peak was mostly due to the kinetic energy distribution of the pions. The energy spectrum of events rejected by the $\Delta\chi^2$ cut was used to represent the background peak at 4.1 MeV. Since the events rejected by the $\Delta\chi^2$ cut had a bias due to the requirement of >2 MeV muon energy, the peak position and width were slightly different from those of the remaining events. The bias was compensated by multiplying the background peak by a unit Gaussian function with its center shifted by 0.1 MeV. The amplitude of the background peak and the width of the unit Gaussian were free parameters of the fit. A quadratic function was used for the π DIF background.

Fig. 4 shows the fit using the two shapes described above. The fitting window of -4.0 to 3.5 MeV resulted in $\chi^2/ndof = 1.39$; there is some deviation above 2 MeV due to a small remaining mismatch in the width and peak position.

The signal peak in the region $T_\mu < 1.2$ MeV was assumed to be a Gaussian; the width was scaled by the square root of the energy from that of the 4.1 MeV peak, and the offset was estimated from the pion-only peak (to represent a peak at 0 MeV) obtained from an 80-ns integration window with a late muon pulse. The signal peak energy was varied from 0.0 MeV to 1.3 MeV with 0.05 MeV steps.

Fig. 5 shows the signal amplitudes, with statistical errors, normalized to that of the 4.1 MeV peak (without the two-pulse requirement) after the acceptance correction of 1.06 for the Z-vertex cut; the distribution of the events in the 4.1 MeV peak was wider due to the longer muon range. Since no significant signal beyond the statistical fluctuation was observed, 90% CL upper limits on the neutrino mixing parameter $|U_{\mu i}|^2$ were obtained according to the Bayesian procedure assuming a positive peak amplitude with a Gaussian probability distribution [12]. The full black circles in Fig. 1 show the result for $0 < T_\mu < 1.2$ MeV.
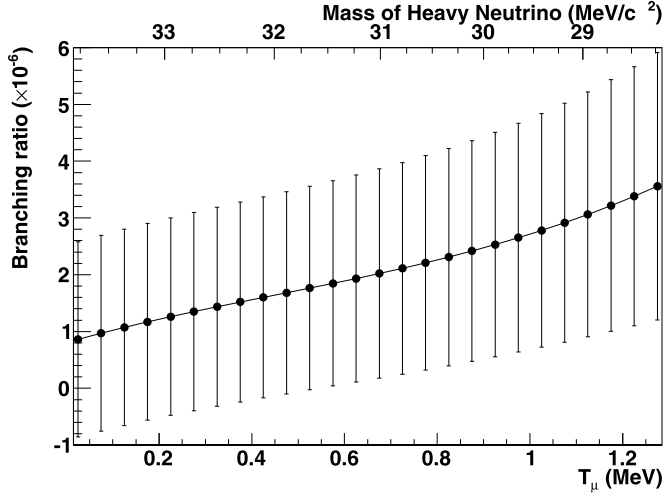
Fig. 5. Normalized amplitudes (branching ratio) vs kinetic energy with statistical errors ($\pm 1\sigma$) after the Z-vertex acceptance correction. The upper scale shows m_H. Note: The step size is much smaller than the peak width.

5. Analysis of the region above 1.2 MeV

In this analysis, the energy of the second pulse in the $\pi^+ \to \mu^+ \to e^+$ decay in B3 was used. The largest background was accidental background originating from decay of an "old" muon from an earlier pion or muon residing near B3 to a positron, giving a second or third pulse; some accidental background was already suppressed by the requirement of no additional coincident activity in the detectors. Radiative pion decay $\pi^+ \to \mu^+ \nu \gamma$ (branching fraction, 2×10^{-4} [27]) was about one tenth of the accidental background in the previous experiment [11].

Events with three separate pulses in B3 were selected in this analysis. Fig. 6 shows energy spectra of the second pulse with consecutive cuts described below. In order to clearly separate the positron pulse from the muon pulse, events with a late positron signal, firing T1 and the calorimeter in the positron time region $200 < t_{T1} - t_{B1} < 500$ ns, were selected. The second pulse was required to be within 80–150 ns with respect to the first pulse (pion stop). With this cut the energy variation due to the overshoot of the first pulse was minimized to <0.16 MeV (a negligible level in terms of resolution).

The comparison of the pulse height and the integrated charge (-20 to 20 ns) of the first pulse identified early pion decays in which the muon pulse merges into the first pulse and a positron pulse is recognized as the second. The kink angle and Z-vertex cuts reduced the contribution of πDIF. After these cuts, the radiative pion decay $\pi^+ \to \mu^+ \nu \gamma$ was the major source of background. The total number of events used for the search in the region $T_\mu > 1.2$ MeV was 9×10^6.

5.1. Fit

The background shape for radiative pion decay was generated by MC [25] with the selection cuts, and the amplitude was a free parameter in the fit. A constant term (not in the final fit) was also added as a free parameter to represent other potential backgrounds, but it was always consistent with zero. The peak at 4.1 MeV was fitted with a Gaussian with the width, amplitude and position as free parameters. The acceptance losses due to the selection requirements were common to those of the peak at 4.1 MeV except for the pulse-detection logic which depended on the amplitude of the pulse (note the sharp drop around 1 MeV). This acceptance was estimated by comparing the observed positron energy
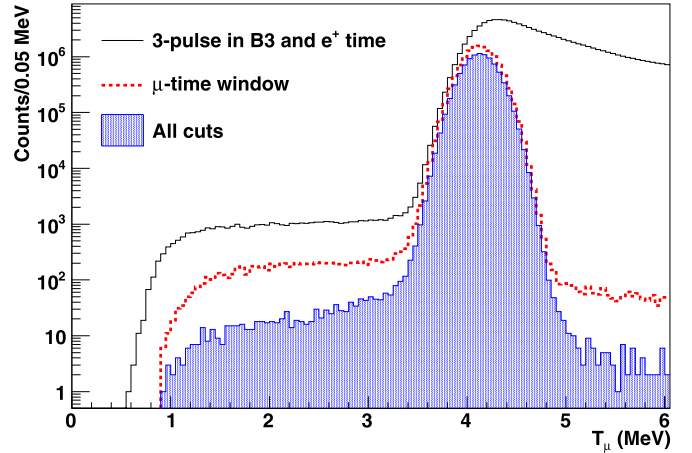

Fig. 6. Energy spectra of the second pulse. The black histogram is for positrons in the 200–500 ns window as the third pulse, the dotted red histogram with the time window cut of 80–150 ns for the second pulse, and the shaded blue histogram with all cuts.
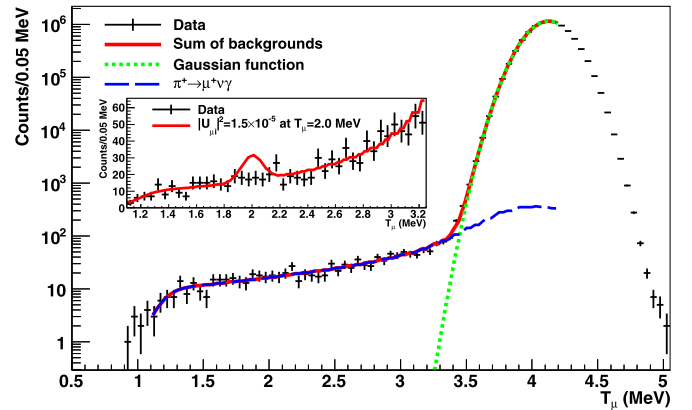

Fig. 7. Fit results for the region $T_\mu > 1.2$ MeV. Data are shown by the black crosses with statistical errors. The solid red line is for the fit results The dotted green line is for the 4.1 MeV Gaussian peak and the dashed blue line for the radiative decay background. In the insert, the red line indicates a hypothetical signal at 2 MeV for $|U_{\mu i}|^2 = 1.5 \times 10^{-5}$.

spectrum with the MC positron spectrum which was not affected by the effects of the detection logic. Since the background events were also affected by the pulse detection logic, the fitting functions of the background and the signal were multiplied at the time of fit by this empirical acceptance function.

A fit in the energy region $1.1 < T_\mu < 4.2$ MeV with a no-signal assumption provided a total $\chi^2 = 68$ with 58 degrees of freedom. The largest deviations were in the region above 3.4 MeV. Fig. 7 shows the data in black and the result of the background fit in the solid red line. The peak at 2 MeV (the red line) in the insert indicates a hypothetical signal for $|U_{\mu i}|^2 = 1.5 \times 10^{-5}$.

For the search for additional peaks, the signal function, a Gaussian with the width scaled by the square root of the energy from that of the 4.1 MeV peak, was added to the fitting function. The signal peak was shifted in 0.05 MeV steps for the search. The amplitude of the signal peak was an additional free parameter of the fit. No significant excess above statistical fluctuations was observed. The amplitudes of hypothetical peaks normalized to the 4.1 MeV peak, with the Z-vertex acceptance correction, are shown in Fig. 8. The systematic uncertainty was estimated to be less than 5% and neglected. Since we did not see a significant excess in the signal amplitudes, a 90% CL upper limit on the mixing matrix ele-
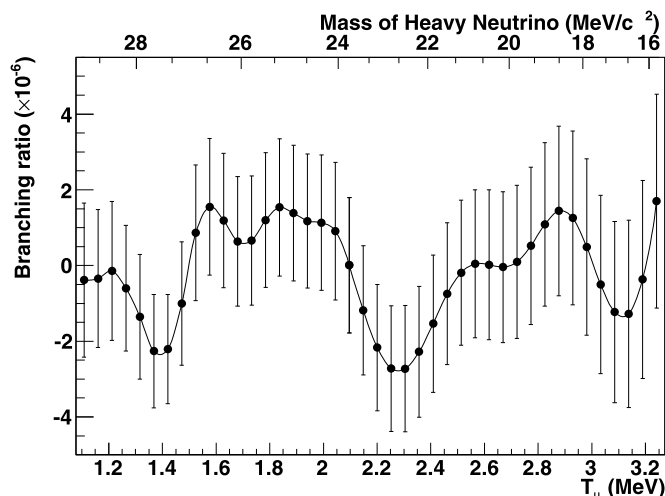
Fig. 8. Normalized amplitudes of the second pulse (branching ratio) vs kinetic energy with statistical errors ($\pm 1\sigma$). The upper scale shows m_H.

ment $|U_{\mu i}|^2$ was set for each neutrino mass. The open black circles for $1.1 < T_\mu < 3.3$ MeV in Fig. 1 show 90% CL upper limits for $|U_{\mu i}|^2$.

6. Conclusion

Additional peaks due to heavy neutrinos were searched for in $\pi^+ \to \mu^+ \nu$ decay at rest and no evidence was observed. Upper limits on the neutrino mixing parameter $|U_{\mu i}|^2$ were obtained for the region $0 < T_\mu < 3.3$ MeV, which corresponds to $15.7 < m_H < 33.8$ MeV/c^2. The improvement factors were approximately an order of magnitude compared to the previous searches [11–13].

Acknowledgements

References

[1] M. Drewes, Int. J. Mod. Phys. E 22 (2013) 1330019.
[2] L. Canetti, M. Drewes, M. Shaposhnikov, New J. Phys. 14 (2012) 095012.
[3] M. Viel, *et al*, Phys. Rev. D 71 (2005) 063534.
[4] O. Ruchayskiy, A. Ivashko, J. Cosmol. Astropart. Phys. 1210 (2012) 014.
[5] G.B. Gelmini, A. Kusenko, V. Takhistov, arXiv:1906.10136, 2019.
[6] T. Asaka, S. Blanchet, M. Shaposhnikov, Phys. Lett. B 631 (2005) 151–156.
[7] H. Ishida, M. Kusabe, H. Okada, Phys. Rev. D 90 (2014) 083519.
[8] J. Huang, A.E. Nelson, Phys. Rev. D 88 (2013) 033016.
[9] G. Gelmini, et al., J. Cosmol. Astropart. Phys. 0810 (2008) 029.
[10] B. Batell, et al., Phys. Rev. D 97 (2018) 075016.
[11] R. Abela, et al., Phys. Lett. B 105 (1981) 263.
[12] D.A. Bryman, T. Numao, Phys. Rev. D 53 (1996) 558.
[13] M. Daum, et al., Phys. Rev. D 36 (1987) 2624.
[14] M. Daum, et al., Phys. Rev. Lett. 85 (2000) 1815–1818.
[15] R.S. Hayano, et al., Phys. Rev. Lett. 49 (1982) 1305.
[16] A.V. Artamonov, et al., Phys. Rev. D 91 (2015) 052001;
     A.V. Artamonov, et al., Phys. Rev. D 91 (2015) 059903.
[17] E. Cortina Gil, et al., NA62 Collaboration, Phys. Lett. B 778 (2018) 137.
[18] R.E. Shrock, Phys. Rev. D 24 (1981) 1232.
[19] A. Aguilar-Arevalo, et al., Phys. Rev. Lett. 115 (2015) 071801.
[20] A. Aguilar-Arevalo, et al., Nucl. Instrum. Methods A 791 (2015) 38–46.
[21] A. Aguilar-Arevalo, et al., Nucl. Instrum. Methods A 609 (2009) 102–105.
[22] Components borrowed from this experiment G. Blanpied, et al., Phys. Rev. Lett. 76 (1996) 1023.
[23] I-H. Chiang, et al., IEEE Trans. Nucl. Sci. NS-42 (1995) 394.
[24] Y. Igarashi, et al., IEEE Trans. Nucl. Sci. NS-52 (2005) 2866.
[25] S. Agostinelli, et al., GEANT4 collaboration, Nucl. Instrum. Methods A 506 (2003) 250.
[26] A. Aguilar-Arevalo, et al., Phys. Rev. D 97 (2018) 072012.
[27] G. Bressi, et al., Nucl. Phys. B 513 (1998) 555.